RSC Advances

ROYAL SOCIETY OF CHEMISTRY

www.rsc.org/advances

Preparation of Y-doped ZrO_2 coatings on MnO_2 electrodes and their effect on electrochemical performance for MnO_2 electrochemical supercapacitor

Yuqing Zhang[ab1,] Yufeng Zhai

[a] *School of Chemical Engineering and Technology, Tianjin University, 300072, Tianjin, P. R. China.*

[b] *Collaborative Innovation Center of Chemical Science and Engineering (Tianjin), Tianjin 300072, P R China*

Abstract: To enhance the cycling stability and conductivity of manganese binoxide (MnO_2) electrodes for supercapacitors, yttrium(Y) doped zirconia (ZrO_2) (denoted as Y/ZrO_2) are coated on MnO_2 electrodes as supercapacitors electrodes (Y/ZrO_2@MnO_2 eletrodes), so protecting the MnO_2 electrodes in electrolytes and enhancing the electrochemical performance of MnO_2 electrodes in sodium sulfate electrolytes. Y/ZrO_2@MnO_2 eletrodes are characterized by scanning electron microscope (SEM), transmission electron microscope (TEM), energy dispersive xray spectrom (EDX) and XRD analysis. The electrochemical properties of electrodes are tested and analyzed by galvanostatic charge/discharge tests, cyclic voltammetry (CV) and electrochemical impedance spectroscopy (EIS). The Y/ZrO_2@MnO_2 electrodes get a specific capacity of 282.1 F g^{-1} with a specific capacity loss of only 6.3% after 100 cycles at the current density of 50 mA g^{-1}.The results show that MnO_2 particles are successfully deposited by Y-doped ZrO_2 while the the Y/ZrO_2@MnO_2 electrodes display better cycling stability and capacity performance. Therefore, Y-doped ZrO_2 coating is the potential choice to improve the cycling stability and conductivity of MnO_2 electrode.

Keywords: Y-doped ZrO_2 coating; MnO_2; Supercapacitors; Specific capacity; Cycling stability.

* Corresponding author. Phone: +86-22-27890470; fax: +86-22-27403389;

E-mail address: zhangyuqing@tju.edu.cn

1. Introduction

After entering 21st century, with increasing consumption of fossil fuels for the development of the economy, the environment pollution and energy crisis have become the most important problems that we must deal with. Therefore, there is a great need of looking for renewable and sustainable energy sources and developing technologically advanced devices for energy conversion and storage[1-4]. In recent years, electrochemical supercapacitors (ESs), as a new sort of efficient device for energy conversion and storage, have caused the extensive concern because of their high power density, fast charge and discharge rate, better cycling stability, and longer life-cycle[1,2]. These properties and characteristics make ESs to be applied in many domains, such as electric vehicles, computer, electrochemical power source, military, power distribution system, etc[5-7]. Therefore, supercapacitors are expected to become a novel energy resource to solve the problem about energy storage and environmental pollution.

The electrochemical properties of supercapacitors, such as specific capacity and cycling stability, intimately depend on the electrode materials[2]. Thus, improving the electrochemical performance of electrode materials is an effective strategy to enhance the electrochemical properties of supercapacitors. Generally, various materials for electrodes of supercapacitors such as carbonaceous materials, conducting polymers and transition-metal oxides have been researched. Among these materials, MnO_2, as a sort of transition-metal oxides, is considered as a promising alternative class of materials for electrochemical supercapacitors, for its superior characteristics such as large theoretical specific capacity (1370 F g^{-1}), environmental safety, low toxicity and natural abundance, as well as low cost[8-10]. In spite of all of the superiorities, commercial applications of supercapacitors based on MnO_2 electrode have not been implemented mostly due

to some existing drawbacks about MnO_2 as follows. Firstly, partial dissolution of MnO_2 electrode in the electrolyte happens spontaneously during cycling, leading to the fading capacity[2,11]. Secondly, poor electronic conductivity and ionic conductivity result in large resistence of MnO_2 electrode in supercapacitors[12]. Hence, it is a key task for researchers to solve these disadvantages of MnO_2 material mentioned above.

Among these drawbacks of MnO_2 electrode material mentioned above, the partial dissolution in the electrolyte is the most prominent issue and draws great attention of researchers. Pang and Anderson[13,14] utilized sol-gel method to prepare thin-film MnO_2 electrode, the result of test indicating that more than 10% capacity was lost after 1500 cycles , in 0.1mol L^{-1} Na_2SO_4 electrolyte, at a scanning rate of 50 mV s^{-1}. Reddy et al.[15] prepared MnO_2 electrode, at a sweep rate of 5 mV s^{-1}, suffering more than 50% capacity loss after 800 cycles. Recently, Hsieh et al[13] also reported the capacity fading of electrochemical capacitors based on the $MnO_2 \cdot nH_2O$ electrodes, ranging from 5% to 30% in 1000 cycles, which was close to current rate and binder content. Moreover, it has been reported that the protective coatings on the electrodes surface are an effective strategy to improve the cycling stability of the electrode and enhance its electrochemical properties[16]. Walz et al[17] deposited nanoporous silica coating on solid barium ferrate particles and obviously enhanced its stability, comparing to the uncoated materials. Licht et al have used ceramic material of zirconia (ZrO_2) as protective coatings on the K_2FeO_4 electrodes, and their investigation results indicate that the ZrO_2 coating effectively enhances the stability of these electrodes, simultaneously improves the energy storage capacity of super-iron batteries[18,19]. Nevertheless, as we all know, ZrO_2 can form cubic, tetragonal, and monoclinic phases or orthorhombic phases. Among these phases, the cubic form has caused the extensive concern

attributed to its high conductivity, excellent thermal stability, mechanical properties, chemical resistance, and oxygen conductivity. In spite of all of the superiorities, the stability of the cubic form at room temperature is not satisfactory. Therefore, the stabilization of cubic form at room temperature is very necessary[20,21]. It is reported that doping Y to ZrO_2 can stabilize cubic of ZrO_2 at room temperature; meanwhile the conductivity of cubic ZrO_2 at room temperature can be improved as well[22]. In addition, Zhang et al[23,24] successfully investigated and developed Y-doped zirconia coatings on K_2FeO_4 particles, significantly enhancing the stability and conductivity of the coated K_2FeO_4 electrodes and provided a good strategy for our further research.

Based on the previous work and investigation above, it is necessary to research and develop a novel sort of electrode materials for supercapacitors. Therefore, in order to enhance the cycling stability and conductivity of manganese binoxide (MnO_2) electrodes for supercapacitors in this paper, yttrium (Y) doped zirconia (ZrO_2) (denoted as Y/ZrO_2) are coated on MnO_2 electrodes as supercapacitors electrodes ($Y/ZrO_2@MnO_2$ eletrodes), so protecting the MnO_2 electrodes and enhancing the electrochemical performance of MnO_2 electrodes in sodium sulfate electrolytes. And then their structure and electrochemical performance were observed and researched through SEM, TEM, EDX, galvanostatic charge/discharge test, CV and EIS.

2. Experimental

2.1 Materials

Zirconium oxychloride octahydrate ($ZrOCl_2 \cdot 8H_2O$) (AR grade, ≥99.0%), ammonia water ($NH_3 \cdot H_2O$) (AR grade, 25%-28%), and cetyltrimethyl ammonium bromide (CTAB) (AR grade, 99.0%) were purchased from Tianjin GuangFu fine chemical research institute. Manganous sulfate ($MnSO_4 \cdot H_2O$) (AR grade, ≥99.0%), ethanol absolute (C_2H_5OH) (AR grade, ≥99.7%), and sodium

sulfate (Na_2SO_4) (AR grade, ≥99.0%) were supplied by Tianjin Guangfu Fine Chemicals Co., Ltd. Potassium permanganate ($KMnO_4$) (AR grade, ≥99.0%) and yttrium nitrate ($Y(NO_3)_3·6H_2O$) (AR grade, ≥99.0%) were obtained from Tianjin Jiangtian chemical Co., Ltd. Acetylene black (AR grade, ≥99.0%, Tianjin Jinqiushi Chemical Co., Ltd.), Poly vinylidenedi fluoride (PVdF) (AR grade, ≥99.0%, Chengdu Chenguang Research Institute of Chemical Industry), nickel foam, and N-methyl pyrrolidone (NMP) (AR grade, ≥99.0%, Tianjin Bo di Chemical Co., Ltd.) were obtained and used as-received.

2.2 Preparation of $Y/ZrO_2@MnO_2$ electrodes

2.2.1 Preparation of MnO_2 particles

A certain amount of CTAB was dissolved in 67 ml deionized water under magnetic stirring. After CTAB powders were completely dissolved, 0.6320g $KMnO_4$ granules were added into the CTAB solution, which was kept stirring for 30 minutes. Then the $MnSO_4$ aqueous solution (1.014g $MnSO_4·H_2O$ powders dissolved in 100 ml deionized water) was dropped into $KMnO_4$ solution by a dropping funnel at a speed of 2 drops per second under powerful magnetic stirring. The whole process was kept at constant temperature of 30℃. The products were collected by centrifugation, washed by ethyl alcohol and deionized water for several times and dried at 60 ℃ in the air for 6 hours.

2.2.2 Preparation of $Y/ZrO_2@MnO_2$ electrodes

Firstly, a certain amount of $ZrOCl_2·8H_2O$ and $Y(NO_3)_3·6H_2O$ was added into 100 ml deionized water in a 250 ml conical flask, kept stirring for 10 minutes after the powders were completely dissolved. Then a certain amount of CTAB was added into the solution. After complete dissolution, the solution was kept stirring for 30 minutes. Finally, 1 g prepared MnO_2 particles

were added and then handled with ultrasonic treatment for 30 minutes. After that, the dilute ammonia solution was dropwise added into the prepared solution above slowly by a dropping funnel. The solution pH value was adjusted from 8 to 9 and then the solution was kept stirring for several hours. The whole process is under constant 30 ℃. Finally, the products were collected by centrifugation, washed by ethyl alcohol and deionized water for several times and dried for 6 hours at 60 ℃ in the air. After above reactions, the dried particles were calcined in the air in pipe furnace at 450 ℃ for 3 h and the $Y/ZrO_2@MnO_2$ powders were obtained.

2.3 Fabrication of electrodes

The electrodes for evaluating the electrochemical properties were fabricated by mixing $Y/ZrO_2@MnO_2$ (80 wt%) sample with acetylene black (10 wt%) and PVdF (10 wt%) in a beaker. Then moderate amount of NMP was added into the electrode material to form slurry. After that, the slurry was coated (coating area: 1×1 cm^2) on a nickel foam (1.8 mm, washed by ethyl alcohol under sonication for 1h). Next, the electrodes were dried at 60 ℃ for 3h under vacuum (vacuum degree: $\geq$ 0.08 MPa), and then pressed at 10 MPa for 10 seconds. Finally, the electrodes were dried at 60 ℃ for 12 h in the air.

2.4 Characterization

2.4.1 SEM analysis

The surface morphologies and structures of the as-prepared samples were observed using a scanning electron microscope (SEM, Hitachi S-4800, Japan).

2.4.2 TEM analysis

The surface morphologies and structures of the as-prepared samples were observed using a transmission electron microscopy (TEM, JEOL JEM-2100F, Japan).

2.4.2 EDX analysis

The content of elements in the surface of the as-prepared samples were observed using a Energy dispersive X-ray spectrometer (EDX, Tecnai G2F20 FEI, Netherlands).

2.4.3 XRD analysis

The XRD patterns were recorded using a RINT2000 diffractometer (Rigaku Corporation, Japan) equipped with a CuKα X-ray source. Data were collected in the 2θ range 10-80°.

2.5 Electrochemical tests

Electrochemical tests of the as-prepared electrodes, including the galvanostatic charge/discharge test, the cyclic voltammetry (CV) test, and the electrochemical impedance spectroscopes (EIS) test. All the electrochemical tests were performed using 0.5 mol L^{-1} aqueous Na_2SO_4 solution as the electrolyte at 25 ℃ in this study.

2.5.1 Galvanostatic charge/discharge tests

The galvanostatic charge/discharge tests of electrodes were studied via Land Battery Test System (CT2001A, Wuhan Jinnuo Electronic Ltd., China) in the potential range between 0 and 0.9 A at constant current and in the potential range between 0 and 0.8 V. In this paper, the specific capacity is calculated on the basis of the galvanostatic charge/discharge test curve for testing a single electrode. There are the same two electrodes having identical quality in the process, with a current density of 100 mA g^{-1}.

2.5.2 CV tests

CV tests were performed using a CHI650C electrochemical workstation in a three-electrode configuration, with Y/ZrO_2@MnO_2 particles coated Ni foam, Pt foil (1 × 1 cm^2) and saturated calomel electrode (SCE) as working, counter and reference electrodes, respectively. The potential

voltage range of CV was from -0.5V to 0.5V.

2.5.3 EIS tests

EIS tests were also performed using a CHI650C electrochemical workstation in a three-eletrode configuration as the same as that in the CV tests. And the electrochemical impedance spectra were measured by imposing a sinusoidal alternating voltage frequency of 10^{-2} to 10^{5} Hz.

3. Results and discussion

3.1 Determination of preparation conditions of $Y/ZrO_2@MnO_2$ particles

The electrochemical performances of $Y/ZrO_2@MnO_2$ electrodes are affected by many factors during depositing Y/ZrO_2 coatings on the surface of MnO_2 electrodes. Among those factors, the adding amount of $ZrOCl_2 \cdot 8H_2O$, the doping amount of $Y(NO_3)_3 \cdot 6H_2O$ (the mole ratio of $Y(NO_3)_3 \cdot 6H_2O$ and $ZrOCl_2 \cdot 8H_2O$) (mol : mol), the concentration of CTAB, the reaction time, and the calcination temperature were observed and researched. To determine the fitting preparation conditions of $Y/ZrO_2@MnO_2$ particles, a single factor experiment was used for research and five different levels of every factor were chosen in experiments. Finally, electrodes were prepared using $Y/ZrO_2@MnO_2$ particles to further investigate.

In all the single factor experiments, the specific capacity of produced electrodes mentioned above were evaluated by using the method of galvanostatic charge/discharge test.

3.1.1 Determination of the adding amount of $ZrOCl_2 \cdot 8H_2O$

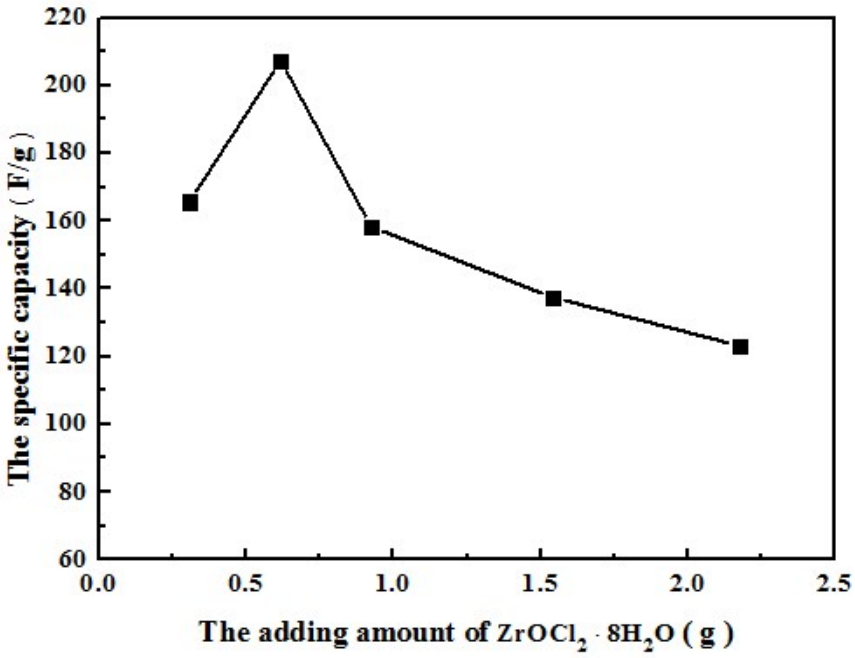

Fig. 1 The effect of adding amount of zirconium oxychloride on the specific capacity of electrodes

Fig. 1 shows that the effect of the adding amount of $ZrOCl_2 \cdot 8H_2O$ on the specific capacity of the electrodes. At the initial stage, the specific capacity of electrodes increases with adding amount of $ZrOCl_2 \cdot 8H_2O$ being increased. When the adding amount of $ZrOCl_2 \cdot 8H_2O$ is 0.6171 g, the specific capacity of electrodes reaches the highest value of 207.3 F g^{-1}. When the adding amount of $ZrOCl_2 \cdot 8H_2O$ is increased continually, the specific capacity of the electrodes is decreased sharply. The reason for the result suggests that: when the adding amount of $ZrOCl_2 \cdot 8H_2O$ is less than 0.6171 g, the electrodes can not be deposited completely, so the coatings are not enough inhibit the fading of specific capacity. And the other hand, the adding amount of $ZrOCl_2 \cdot 8H_2O$ is more than 0.6171 g, the coatings are so thick that they make electrolyte transfer difficultly and even prevent active materials from contacting with electrolyte, leading to the sharp decrease of the specific capacity. In conclusion, 0.6171 g is chosen as the fitting adding amount of $ZrOCl_2 \cdot 8H_2O$.

3.1.2 Determination of the doping amount of $Y(NO_3)_3 \cdot 6H_2O$

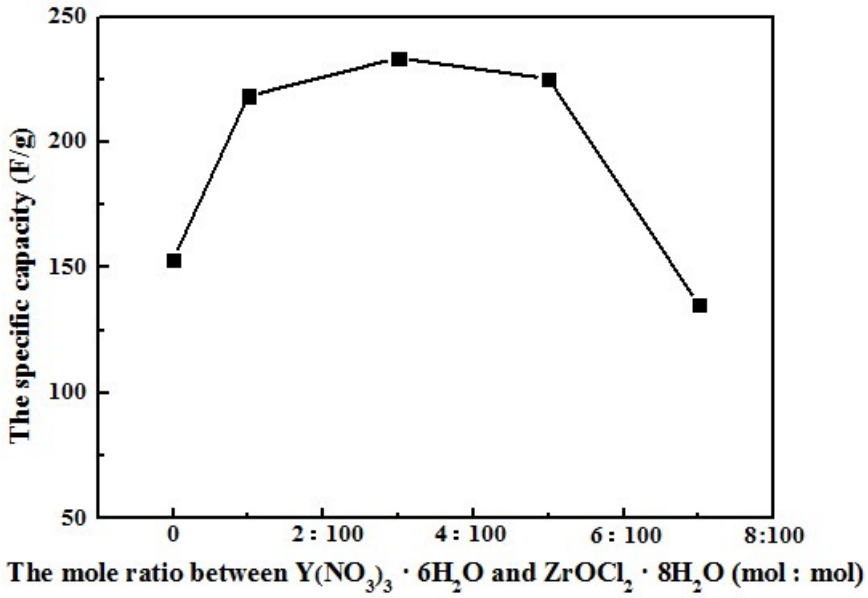

Fig. 2 The effect of yttrium doping amount on the specific capacity of electrodes

The curve in Fig. 2 shows the effect of yttrium (Y) doping amount on the specific capacity of electrodes. At the initial stage, the specific capacity of the electrodes increases with the doping amount of $Y(NO_3)_3 \cdot 6H_2O$ being added. The specific capacity of the electrodes reaches its maximum value of 233.6 F g^{-1} when the mole ratio between $Y(NO_3)_3 \cdot 6H_2O$ and $ZrOCl_2 \cdot 8H_2O$ (mol : mol) is 3:100. Then the specific capacity of the electrodes starts to decrease with the doping amount of yttrium being increased unceasingly. Especially, the mole ratio between $Y(NO_3)_3 \cdot 6H_2O$ and $ZrOCl_2 \cdot 8H_2O$(mol : mol) is more than 5:100, the specific capacity of the electrodes decreases sharply. The reason suggests that： the oxygen vacancies are few in the coating when the doping amount of yttrium (Y) is less, so the resistance of charge transfer is strong, which makes the specific capacity low. With increasing the doping amount of $Y(NO_3)_3 \cdot 6H_2O$, the coatings of the electrodes contain more yttrium (Y), which increases the oxygen vacancies and decreases the resistance of charge transfer. But when the doping amount of $Y(NO_3)_3 \cdot 6H_2O$ is too much, the coatings turn into mixtures of zirconium (Zr) and yttrium (Y), which makes the conductivity in the

coatings of the electrodes decrease seriously. As the result, the resistance of charge transfer grows highly and the specific capacity decreases much. Thereby, the fitting mole ratio between $Y(NO_3)_3 \cdot 6H_2O$ and $ZrOCl_2 \cdot 8H_2O$(mol : mol) is 3:100 .

3.1.3 Determination of the concentration of CTAB

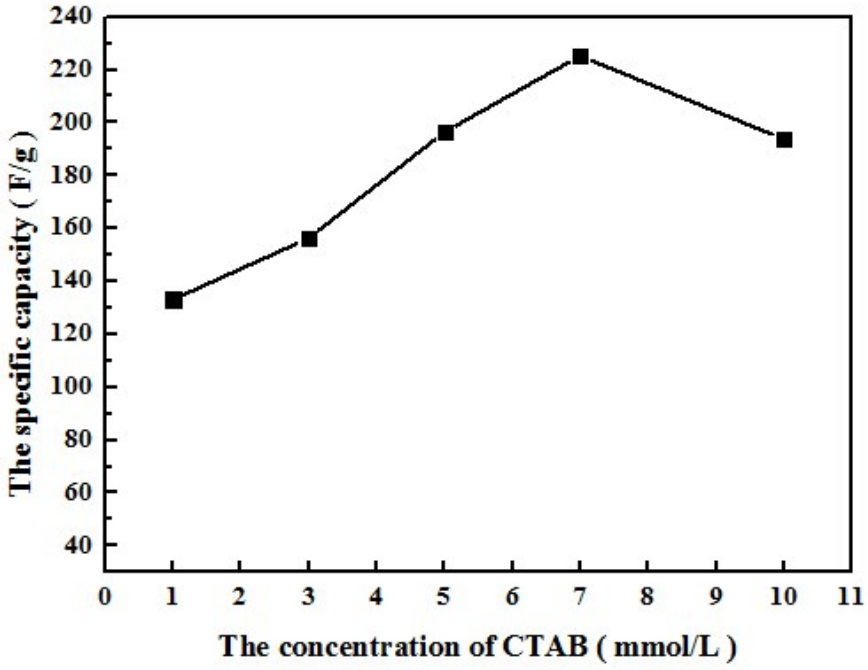

Fig. 3 The effect of the concentration of CTAB on the specific capacity of electrodes

Fig. 3 shows that the specific capacity of the electrodes increases with the increasing of the concentration of CTAB at the initial stage. The electrodes get the highest specific capacity of 225.3 F g^{-1} while the concentration of CTAB is 7 mmol L^{-1}. However, when the concentration of CTAB is more than 7 mmol L^{-1}, the specific capacity begins to decline. This result suggests that: CTAB is added to insure that channels are generated in the inorganic coating shells of the electrodes, which makes active materials easily contact with electrolyte. Channels for electrolyte transfer can not be produced enough if the amount of CTAB is little. So, with adding the concentration of CTAB, the quantity of channels increases continuously, as a result the specific

capacity of the electrodes augments. However, the formation of inorganic coating shells might be prohibited by excess adding amount of CTAB. Therefore, the fitting adding amount of CTAB is 7 mmol L^{-1}.

3.1.4 Determination of the reaction time

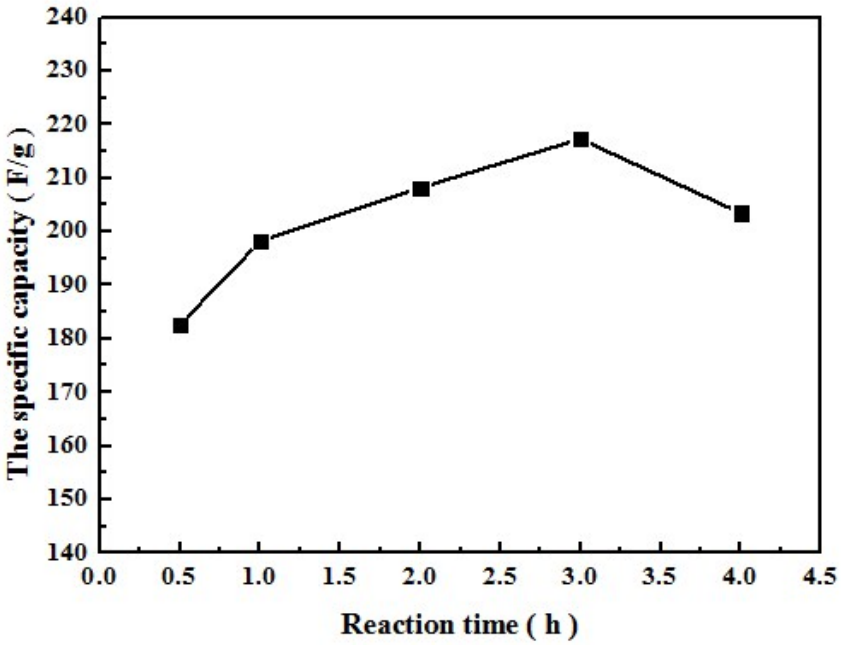

Fig. 4 The effect of reaction time on the specific capacity of electrodes

It is shown in Fig. 4 that the specific capacity increases with the coating reaction time extends. The specific capacity of the electrodes changes slightly when coating reaction time exceeds 2 h. The specific capacity of the electrodes reaches its maximum value of 217.3 F g^{-1} when coating reaction time is 3 h. Then reaction time reaches 4 h, it has a weak influence on the specific capacity, the value of the specific capacity is 203.5 F g^{-1}. The reason suggests that： short reaction time can not enough impel the growth of the inorganic coating shell, in contrast, overlong reaction time will add unnecessary costs. Therefore, the fitting reaction time should be 3 h.

3.1.5 Determination of the calcination temperature

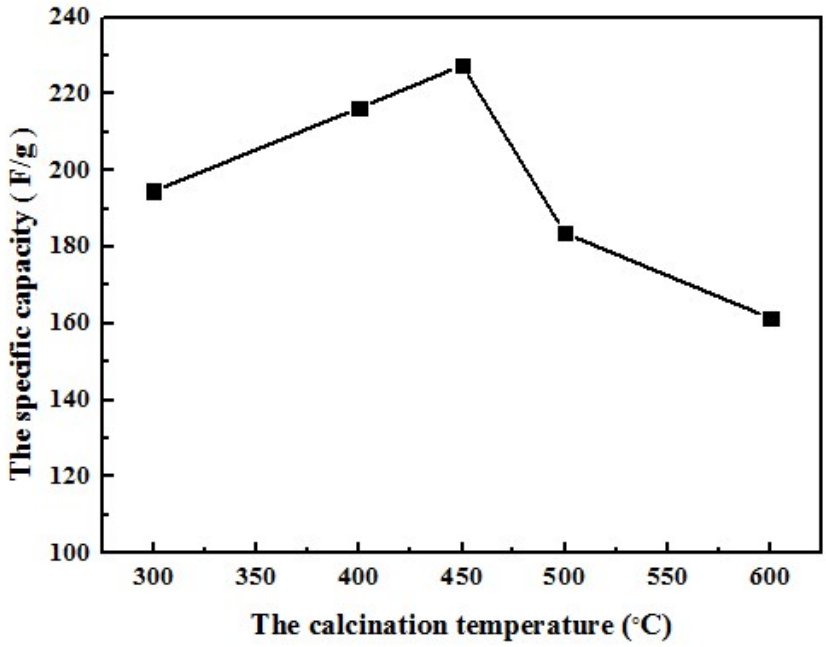

Fig. 5 The effect of different calcination temperatures on the specific capacity of electrodes

As is shown in Fig. 5, the specific capacity of the electrodes increases with rising calcination temperature at the initial stage and reaches the maximum value (227.5 F g^{-1}) at 450 ℃, whereas the specific capacity decreases sharply while calcination temperature exceeds 450 ℃.

Actually, different crystal structures of MnO_2 are formed under different calcination temperatures. When the calcinations temperature is below 300 ℃, MnO_2 is still in amorphous state. However, α-MnO_2 appears when MnO_2 is heated between 400 and 500 ℃ and transforms to α-Mn_2O_3 above 500 ℃[3]. It is reported that if MnO_2 was in amorphous state, it is not stable during cycling as the electrode material, which is adverse to the diffusion of electrolyte. The specific capacity of electrodes decreases sharply when calcination temperature exceeds 450 ℃, because the specific capacity of α-Mn_2O_3 is very little. Therefore, 450 ℃ is adopted as the fitting calcination temperature.

The fitting preparation conditions of Y/ZrO_2@MnO_2 particles are: the mass of $ZrOCl_2 \cdot 8H_2O$

is 0.6171 g, the mole ratio between $Y(NO_3)_3 \cdot 6H_2O$ and $ZrOCl_2 \cdot 8H_2O$ (mol : mol) 3:100, the adding amount of CTAB 7 mmol L^{-1}, the reaction time 3 h, the calcination temperature 450 ℃. Characterizations and electrochemical tests of electrodes prepared under fitting preparation conditions were analyzed and researched as below.

3.2 Characterizations

3.2.1 SEM analysis of materials

The $Y/ZrO_2@MnO_2$ materials for SEM are prepared under the fitting preparation conditions.

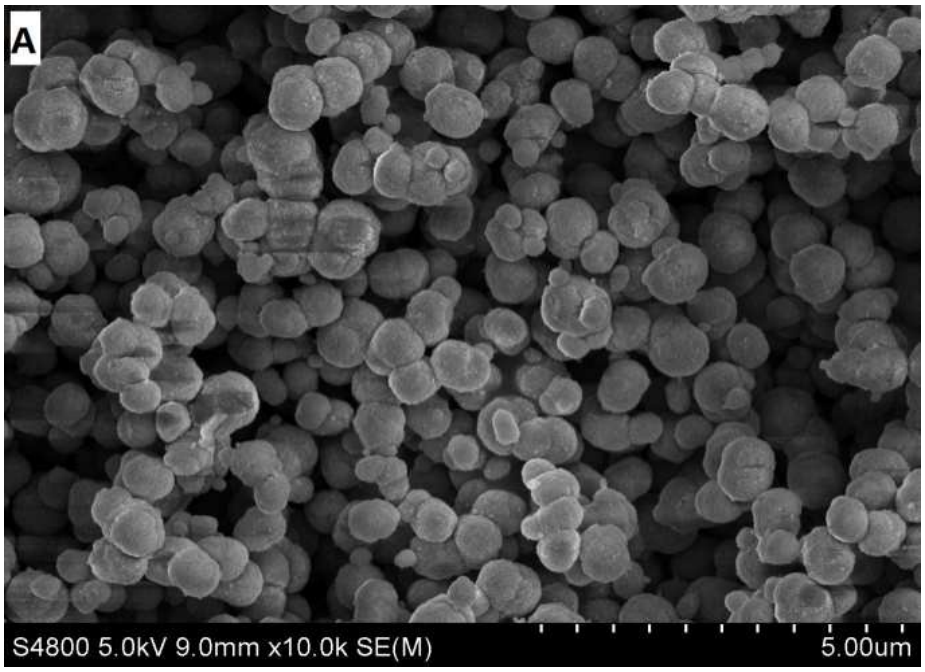

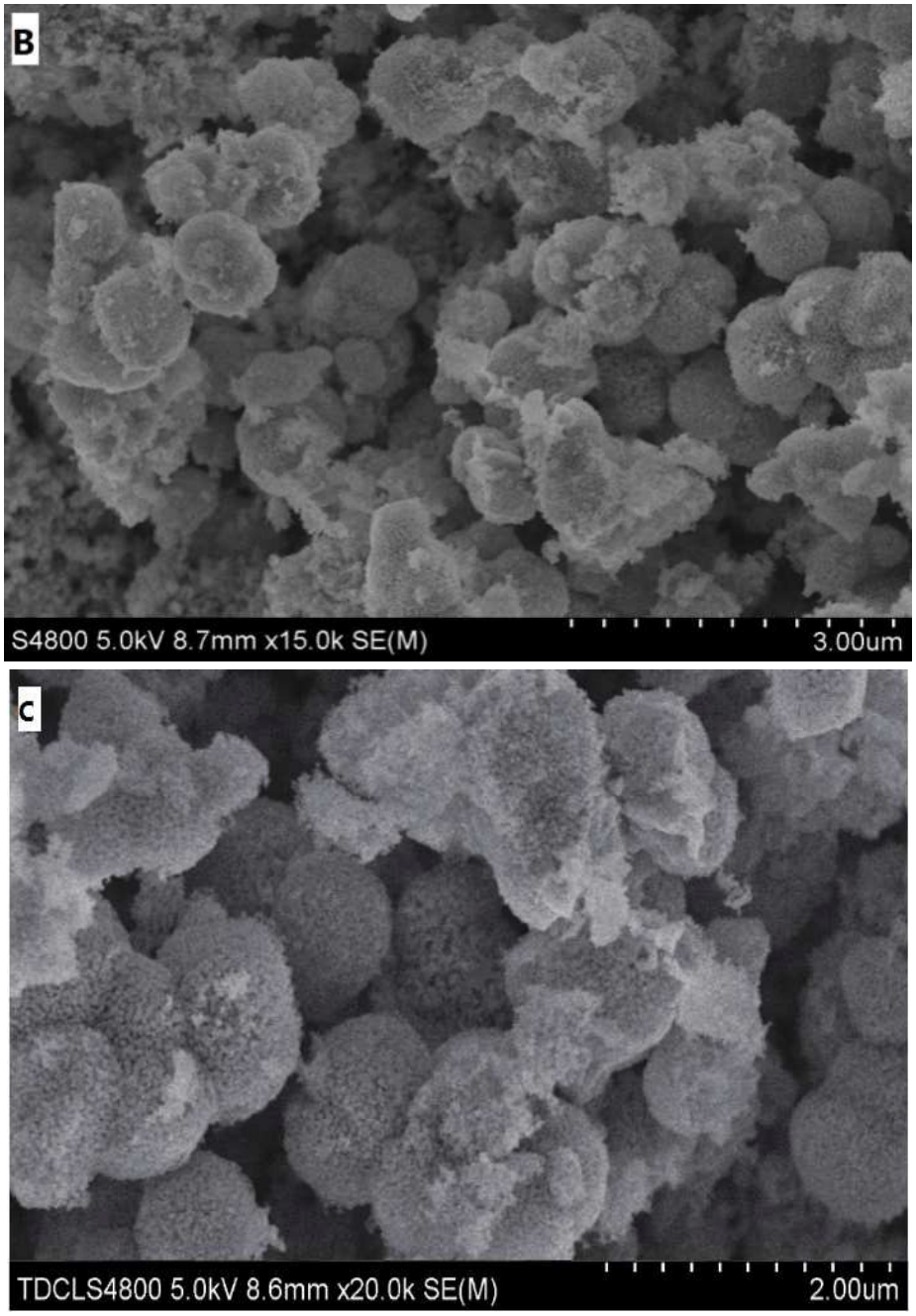

Fig. 6 SEM images: (A) pure MnO2 particles (B) Y/ZrO2@MnO2 particles

(C) Y/ZrO2@MnO2 particles after 5000 cycles

The morphology of pure MnO_2 particles and $Y/ZrO_2@MnO_2$ particles are shown in Fig. 6. SEM images in Fig. 6 (A) reveals that the pure MnO_2 particles perform sphere morphology with smooth surface; meanwhile they have a particle size about 450 nm. Compared to the SEM image

of the pure MnO_2 particles, the surface of $Y/ZrO_2@MnO_2$ particles becomes relatively rough in Fig. 6 (B). These results indicate that MnO_2 materials have been indeed coated by Y/ZrO_2 coatings. Besides, by comparing the images in Fig. 6 (B) and Fig. 6 (C), it is proved that the morphology of Y/ZrO2@MnO2 has no obvious changes after 5000 cycles and the inorganic coating shell increases the cycle stability of the electrode.

3.2.2 TEM and EDX analysis of materials

The $Y/ZrO_2@MnO_2$ materials for TEM and EDX are prepared under the fitting preparation conditions.

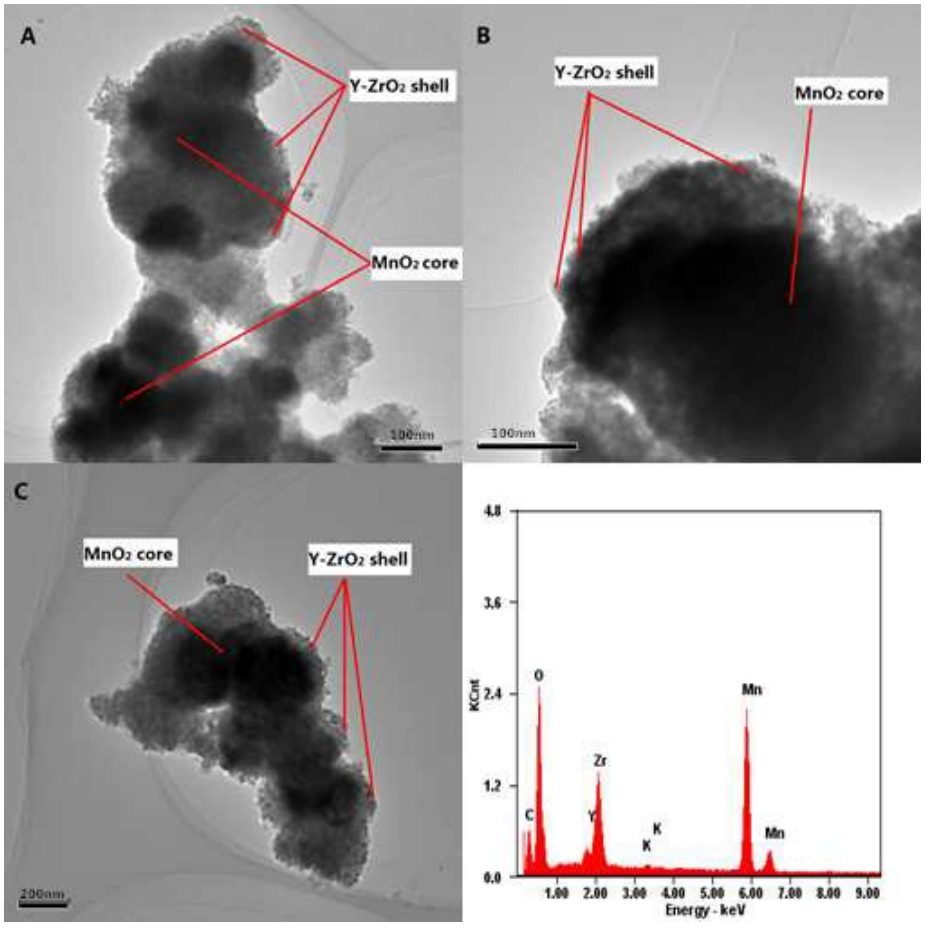

Fig. 7 TEM images and EDX spectrum of $Y/ZrO_2@MnO_2$ particles

TEM images in Fig. 7(A), Fig. 7(B) and Fig. 7(C) show that MnO_2 particles are successfully

by Y/ZrO_2 coatings. In these images, deep color regions stand for MnO_2 particles and gray sections represent Y/ZrO_2 coatings. The thickness of the coating shells is between 20 nm and 50 nm in Fig. 7(B), Fig. 7(A) and Fig. 7 (C). This result is congruent with the result of SEM analysis. Moreover, EDX spectrum indicates that the coating shell includes Y and Zr element, which proves that yttrium is successfully doped into the ZrO_2 coating shells.

3.2.3 XRD analysis of materials

The P-MnO2 and Y/ZrO2@MnO2 materials for XRD are prepared under the fitting preparation conditions: the mass of ZrOCl2·8H2O is 0.6171g, the mole ratio between Y(NO3)3·6H2O and ZrOCl2·8H2O (mol : mol) 3:100, the adding amount of CTAB 7 mmol L-1; the reaction time 3 h; the calcination temperature 450 ℃.

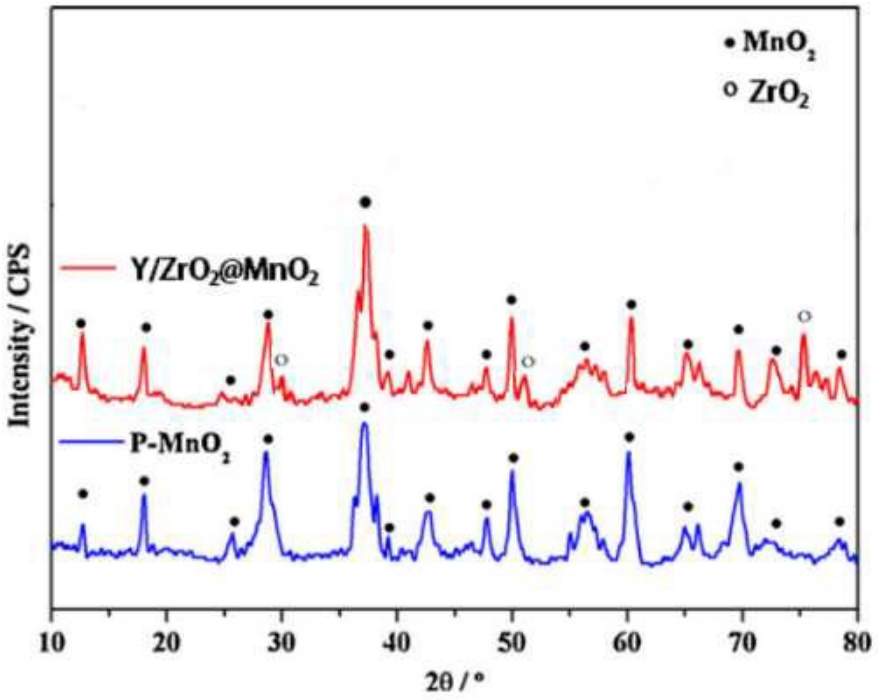

Fig. 8 X-Ray diffraction patterns of different electrode materials

The XRD patterns for P-MnO2 and Y/ZrO2@MnO2 samples are she own in Fig. 8. In the pattern

of the two samples, all diffraction peaks can be indexed to the α-MnO2 according to the JCPDS 44-0141 standard file25. It can be seen from the Fig. 8 that there are some new diffraction peaks appearing and slight deviation of peak position through comparing the patterns of P-MnO2 and Y/ZrO2@MnO2 samples. The new peaks correspond to the ZrO2 according to the JCPDS 07-0343 standard file26. The result indicates the MnO2 succeed to be coated by ZrO2. Meanwhile, no extra peaks pertaining to Y are observed, indicating that no significant changes of the structure occurred during the doping process.

3.3 Electrochemical tests

As indicated by SEM and TEM results, $Y/ZrO_2@MnO_2$ materials is the potential choice application in energy field. To explore the potential applications in electrochemical energy storage, the $Y/ZrO_2@MnO_2$ materials are used to make supercapacitor electrodes, and characterized by galvanostatic charge/discharge test, cyclic voltammetry (CV) and electrochemical impedance spectroscopy (EIS).

3.3.1 Galvanostatic charge/discharge tests of electrodes

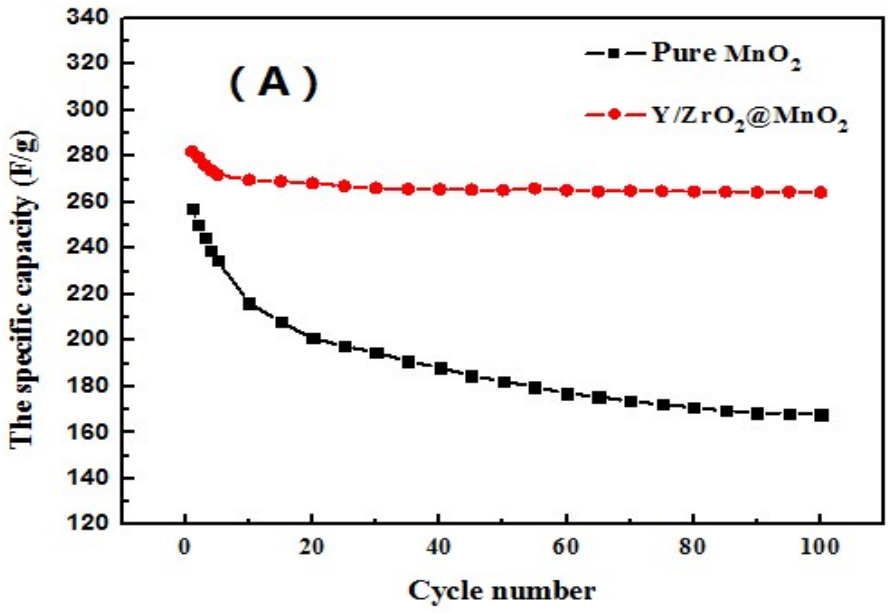

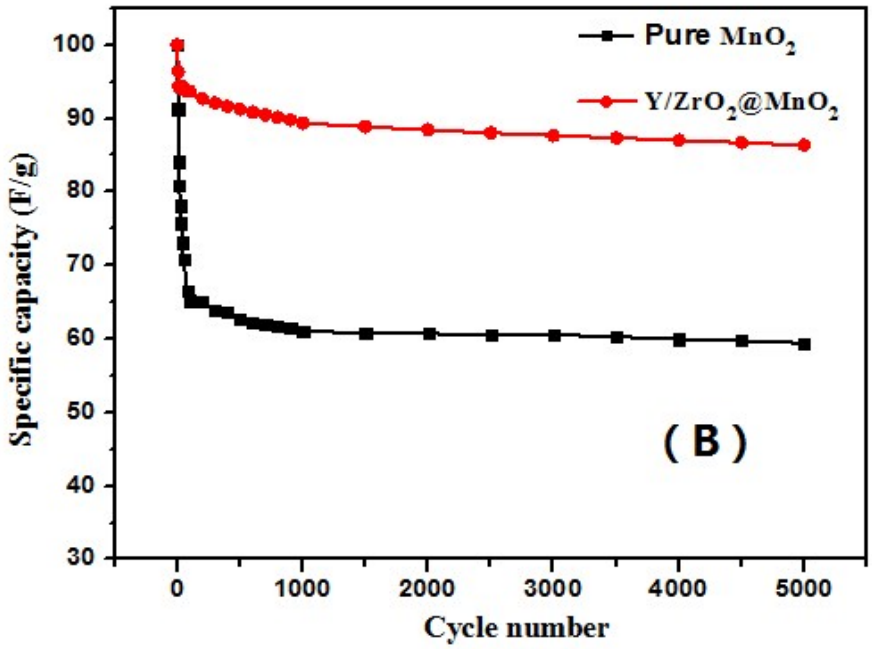

Fig. 9 The effect of cycle number on the specific capacity of electrodes:

(A) 100 cycles (B) 5000 cycles

Cycle life is a key factor to be considered for supercapacitor. Thus, in order to validate the effect of Y/ZrO_2 coatings on the electrodes, the cycle stability tests of pure MnO_2 electrodes and $Y/ZrO_2@MnO_2$ electrodes are carried out under the same current densities of 50 mA g^{-1}. As seen in Fig. 9 (A) and Fig. 9 (B), the specific capacity of pure MnO2 electrodes reaches 257.3 F g-1 at first cycle, and it decreases to 167.9 F g-1 after 100 cycles and 153.0 F g-1 after 5000 cycles, with an overall specific capacity loss of 35% after 100 cycles and 40.5% after 5000 cycles. Under the same current density, the Y/ZrO2@MnO2 electrodes get a specific capacity of 282.1 F g-1 at the initial stage, and it decreases to 264.3 F g-1 after 100 cycles and 243.6 F g-1 after 5000 cycles, with a specific capacity loss of only 6.3% after 100 cycles and 13.6% after 5000 cycles. The two figures indicate that Y/ZrO2 inorganic coating shells increases the specific capacity

and cycle stability of the pure MnO2 electrodes, because Y/ZrO2@MnO2 electrodes shows a larger initial specific capacity and a less attenuation of specific capacity.

The reason suggests that: the protection of Y-doped ZrO_2 coating, which prevents direct contact between MnO_2 electrode and electrolyte, reduces partial dissolution of electrode materials in the electrolyte during cycling test. Simultaneously, the expansion and contraction of MnO_2 crystal lattice is limited by Y-doped ZrO_2 coating, thus the cycle stability of the MnO_2 electrode is improved. Alternatively, the conductivity of ZrO_2 coating is improved by doping yttrium (Y), which decreases surface resistance of ZrO_2 coating on the surface of MnO_2 electrode and charge-transfer resistance of the whole electrode.

3.3.2 CV analysis of electrodes

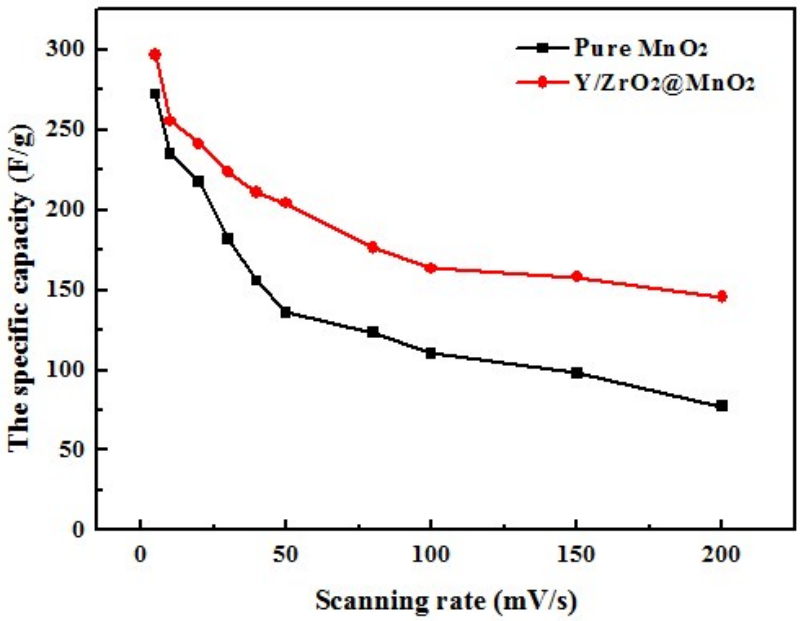

Fig. 10 The effect of scanning rate on the specific capacity of electrodes

The effect of scanning rate on the specific capcacity of pure MnO_2 electrodes and $Y/ZrO_2@MnO_2$ electrodes is shown in Fig. 10. As shown in Fig. 10, when the scanning rate is

5mV s^{-1}, the specific capacity of pure MnO_2 electrode and $Y/ZrO_2@MnO_2$ electrode are 272.4 F g^{-1} and 297.1 F g^{-1}, respectively. With increasing scanning rate, the specific capacity of electrodes decreases sharply. As a result, when the scanning rate is 200mV s^{-1}, the specific capacity of pure MnO_2 electrode and $Y/ZrO_2@MnO_2$ electrode decline to 77.5 F g^{-1} and 145.3 F g^{-1}, and the specific capacity retention ratio are around 28% and 49%, respectively. The result indicates that the Y/ZrO_2 inorganic coating shell increases the specific capacity of pure MnO_2 electrode, and makes the decreasing rate of the specific capacity to be less. The reason suggests that：with the scanning rate increasing, the reaction processes of electrode become faster. Consequently, the immigration and emigration of the electrolyte ion from the electrode can not occur timely. And then, the active materials in the electrode can not have fully reaction, leading to the declination of the specific capacity. Therefore, the Y/ZrO_2 inorganic coating shell increases the overall conductivity of the electrode, indeed.

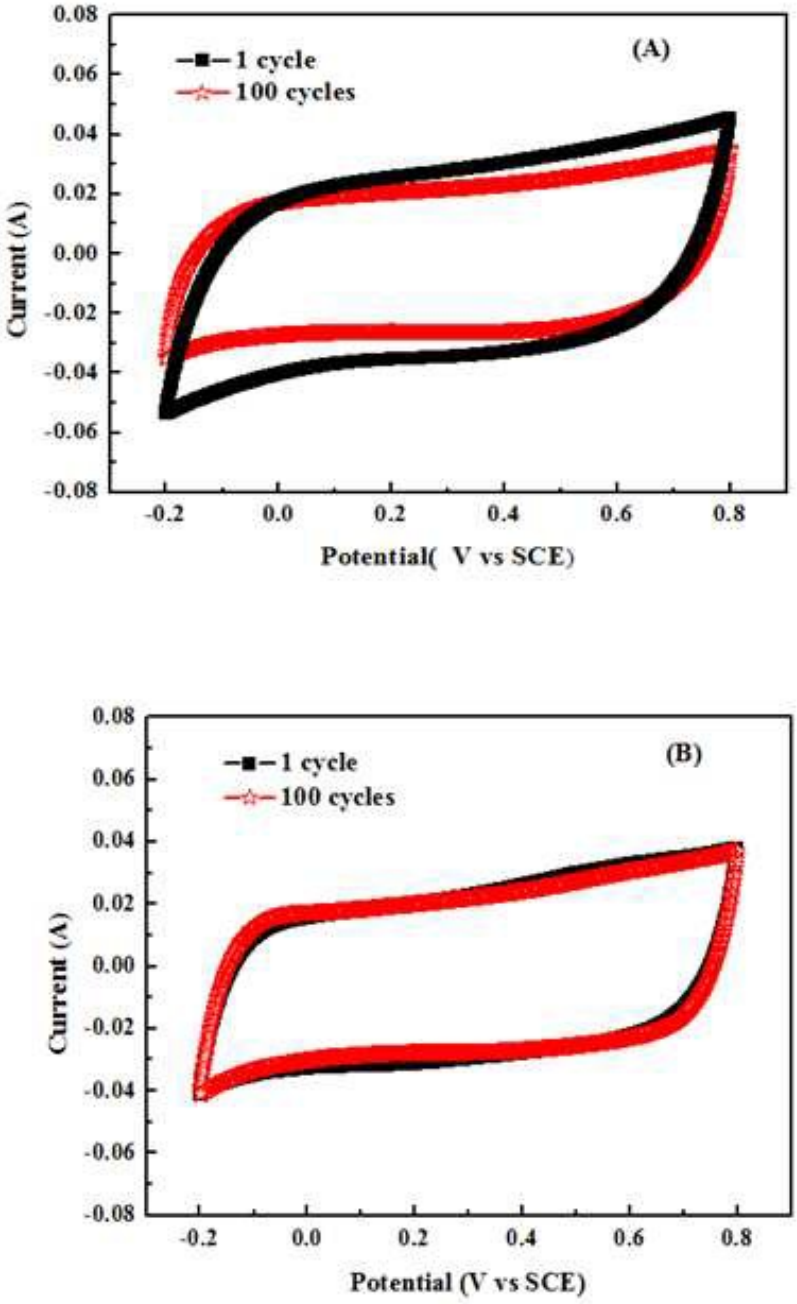

Fig. 11 Effect of cycle number on the cyclic voltammetry property of electrodes:

(A) pure MnO2 electrode (B) Y/ZrO2@MnO2 electrode

The electrochemical properties of the two electrodes are evaluated using CV tests in 0.5 mol L^{-1} Na_2SO_4 solution at the scan rate of 50 mV s^{-1}. As shown in Fig. 11, the test result of the first cycle is compared with that of 100 cycles under same conditions. For pure MnO_2 electrode

evaluated in Fig. 11 (A), although the shape of the CV curves maintain rectangle, the response current decreases obviously after 100 cycles, which implies that the specific capacity of electrode decreases obviously. Then, to compare with the pure MnO_2 electrode, the $Y/ZrO_2@MnO_2$ electrode is shown in Fig. 11 (B), and the CV curves of $Y/ZrO_2@MnO_2$ electrode change little after 100 cycles, which indicates that the response current almost stays the same. Therefore, by comparing the curves of the two electrodes, it is proved that the inorganic coating shell increases the cycle stability of the electrode. This result is congruent with the conclusion of former analysis.

3.3.3 EIS analysis of electrodes

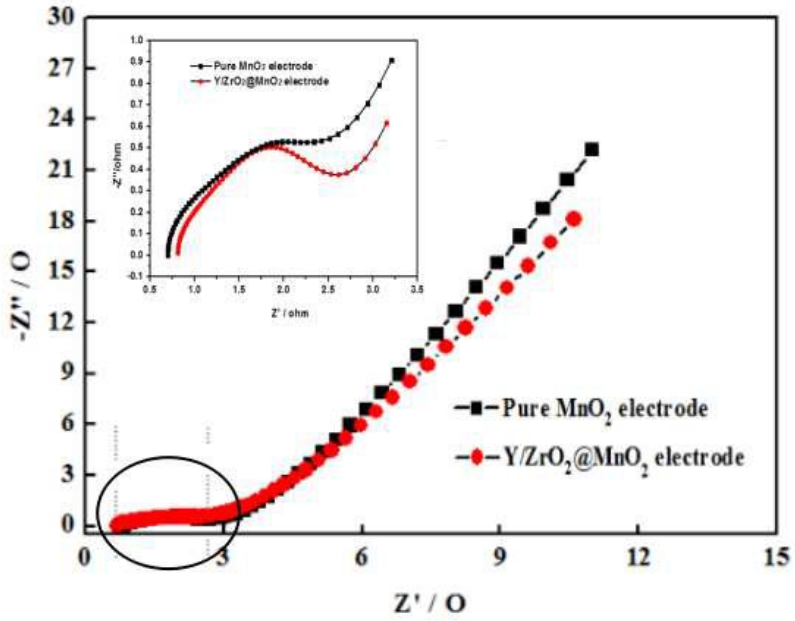

Fig. 12 Nyquist plots of pure MnO2 electrodes and Y/ZrO2@MnO2 electrodes

The Nyquist plots of pure MnO_2 electrodes and $Y/ZrO_2@MnO_2$ electrodes before cycle tests are shown in Fig. 12. In the Nyquist plots, the curve is a depressed arc at high frequency range, corresponding to the charge transfer process. Arc radius stands for the resistance of the charge transfer process and greater radius stands for bigger resistance. The straight line appeared at low frequencies range corresponds to the electrolyte diffusion process. Normally, a higher slope for the

impedance line presents a lower resistance of the electrolyte diffusion process. The two curves display that the charge transfer resistance of pure MnO_2 electrodes is seemingly almost the same to that of $Y/ZrO_2@MnO_2$ electrodes before cycle tests. However, the difference of charge transfer resistance between pure MnO_2 and $Y/ZrO_2@MnO_2$ electrodes materials will be more clearly found when the depressed arc part is enlarged in Fig. 12. It can be concluded that the Y/ZrO_2 coatings indeed decreases the charge transfer resistance of pure MnO_2 electrodes. Then during the electrolyte diffusion process, the slopes of the two lines are approach still, which implies the inorganic coating shell hinders the diffusion of the electrolyte inside the electrode slightly. Therefore, the two curves in Fig. 12 show that the EIS property of the two electrodes is similar to each other before cycle tests.

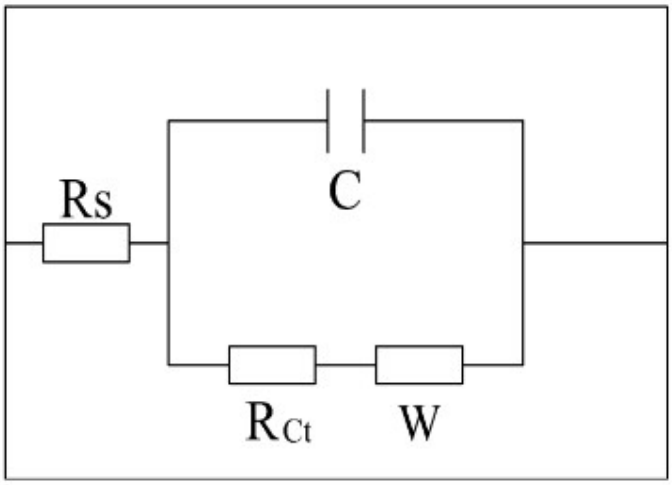

Fig. 13 EIS equivalent circuit of electrodes

Table1

The results of Rs, RCt and W for different electrodes

Types of electrode	Rs / Ω cm2	RCt /Ω cm2	W / Ω cm2
P-MnO2	0.874	1.853	0.241

Y-ZrO2@MnO2	0.842	0.921	0.256

For further investigation, electrodes are described by an equivalent circuit. As seen in Fig. 13, the equivalent circuit is consisted of the electrolyte resistance (Rs), the charge transfer resistance (RCt), the Warburg impedance related to the diffusion in electrolyte (W) and the electrochemical capacitance (C). Based on this equivalent circuit, the values of Rs, RCt and W can be obtained via the software of ZsimpWin, and the corresponding results are listed in Table 1. It can be seen from Table 1, the Rs values of two electrodes are very similar because of the consistent electrolyte. The RCt values of Y-ZrO2@MnO2 electrode are significantly less than the P-MnO2 electrode and the W values of two electrodes are basically the same. These results indicate that the Y-ZrO2 coating reduces the charge-transfer resistance of MnO2 and hardly hinders the diffusion of the electrolyte inside the electrode, which conforms to the Nyquist plots in Fig. 13. The results further demonstrate that the conductivity and the electrochemical properties of the whole MnO2 electrode can be enhanced by Y-doped ZrO2 coating significantly.

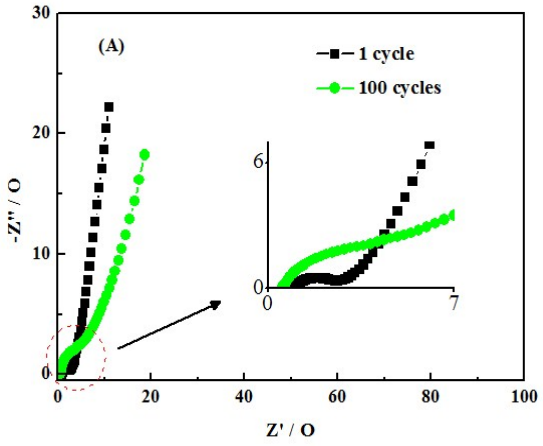

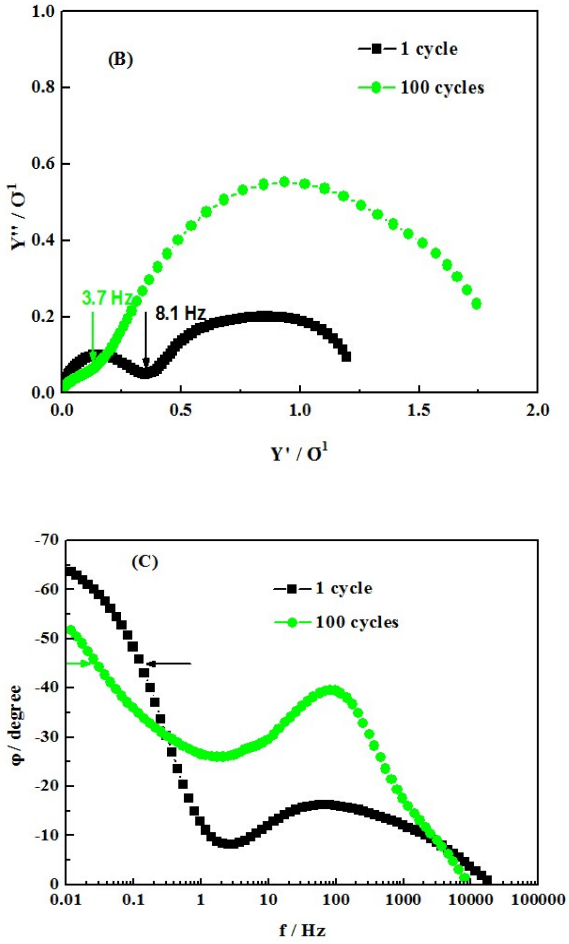

Fig. 14 Effects of cycles number on EIS of pure MnO2 electrodes: (A) Nyquist plot

(B) admittance plot (C) phase angle-frequency plot

The EIS of pure MnO_2 electrodes during electrochemical cycling is shown in Fig. 14 (A).Nyquist plot shows that the radius of depressed arc at high frequencies after 100 cycles is much larger than that after 1 cycle, which implies the resistance of charge transfer process increases with increasing cycle number. The increasing resistance of charge transfer process might be induced by the swells and contracts of MnO_2 lattice during charge-discharge[27], which makes the micro-structure collapse and enlarges internal resistance. Finally, the collapse of the microstructure makes the specific capacity decrease sharply. For the low frequencies in Nyquist

plot, the slope of the line after 100 cycles is lower than that after 1 cycle, which implies that the diffusion resistance of electrolyte inside electrodes greatly increases after 100 cycles. This is because the collapse of microstructure hinders the diffusion of electrolyte. The curve in Fig. 14 (B) shows the admittance plot of pure MnO_2 electrodes. The knee frequency for pure MnO_2 electrodes is reduced from 8.1 Hz (1 cycle) to 3.7 Hz (100 cycles), implying degraded electrochemical response. According to phase angle-frequency plot in Fig. 14 (C), the capacitor response frequency is reduced from 0.12 Hz (1 cycle) to 0.026 Hz (100 cycles). It decreases by 80%, which makes the capacitor response time increases from 8 s to 40 s. As shown in the curves in Fig. 14, the EIS of pure MnO_2 electrodes varies greatly after 100 cycles. The resistance of both charge transfer process and electrolyte diffusion process increases, which reduces the electrochemical response ability and increases capacitor response time.

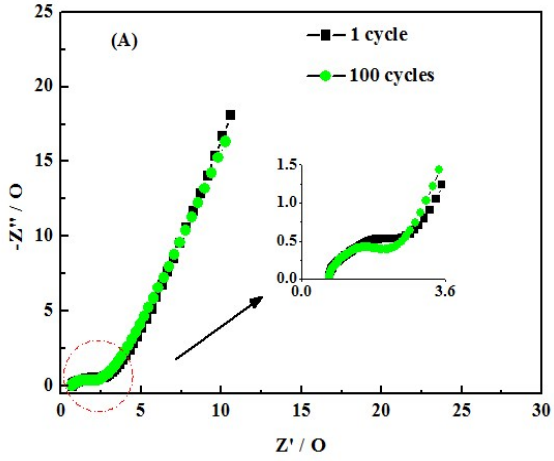

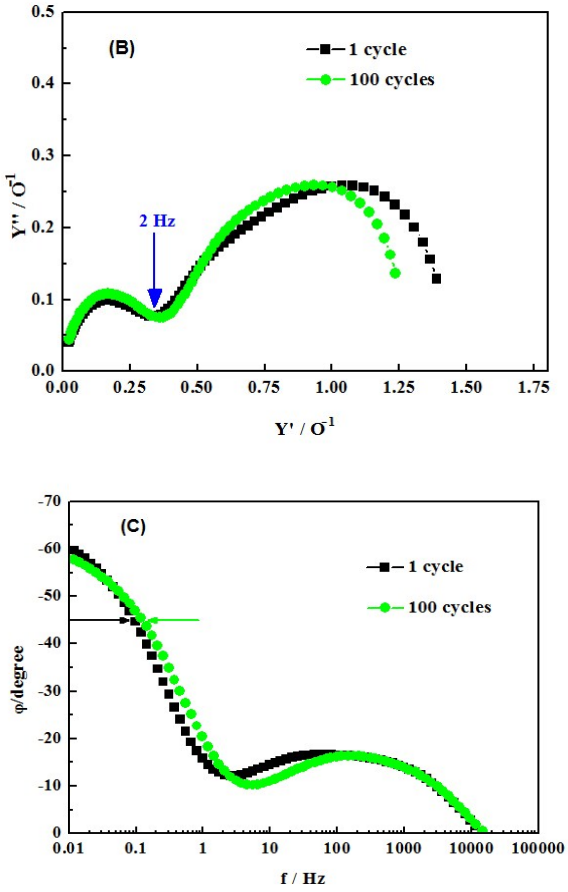

Fig. 15 Effects of cycles number on EIS of Y/ZrO2@MnO2 electrodes: (A) Nyquist plot

(B) admittance plot (C) phase angle-frequency plot

The effect of cycle numbers on the EIS of $Y/ZrO_2@MnO_2$ electrodes is shown in Fig. 15. Nyquist plot in Fig. 15 (A) shows that the radius of depressed arc at high frequencies after 100 cycles is similar to that after 1 cycle, which implies the resistance of charge transfer process during electrodes process mainly remains the same with increasing cycle numbers. Although MnO_2 lattice continually swells and contracts during charge-discharge process, inorganic coating shells effectively protect the microstructure of electrodes, which enhances the cycle stability of the electrodes. For the straight line at the low frequency range, its slope changes little after 100 cycles, indicating the electrolyte diffusion resistance inside the electrodes hardly changes. Fig. 15 (B)

shows the admittance plot of Y/ZrO_2@MnO_2 electrodes. The knee frequency is 2.1 Hz (1 cycle) and 1.9 Hz (100 cycles), which implies the capacitor response ability changes little. According to Fig. 13 (C), the capacitor response frequency is 0.12 Hz (1 cycle) and 0.098 Hz (100 cycles), which only decreases by 19 %. At the same time, capacitor response time increases from 8 s (1 cycle) to 10 s (100 cycles). The curves in Fig. 13 show that the EIS of Y/ZrO_2@MnO_2 electrodes changes little after 100 cycles. The resistance of charge transfer process and electrolyte diffusion process remains largely unchanged, which makes the electrochemical response ability keep the same and the capacitor response time increase little. Compared to the EIS of pure MnO_2 electrodes, the results prove that the inorganic coating shell increases the cycle stability of the electrode indeed.

4. Conclusions

In this paper, a cost-effective and simple strategy is presented to design and fabricate novel Y/ZrO_2@MnO_2 material, to improve the cycle stability and conductivity property of electrode for supercapacitor. The fitting preparation conditions of Y/ZrO_2@MnO_2 particles are: the mass of $ZrOCl_2 \cdot 8H_2O$ is 0.6171 g, the mole ratio between $Y(NO_3)_3 \cdot 6H_2O$ and $ZrOCl_2 \cdot 8H_2O$ (mol : mol) 3:100, the adding amount of CTAB 7 mmol L^{-1}; the reaction time 3 h; the calcination temperature 450 ℃.The results of SEM, TEM, EDX and XRD about electrodes prepared under the fitting preparation conditions show that MnO_2 materials are indeed coated by Y-doped ZrO_2 coatings and Y/ZrO_2@MnO_2 particles possess a core-shell structure. The results of electrochemical tests show that the Y/ZrO_2@MnO_2 electrodes display better cycling stability and capacity performance. Therefore, Y-doped ZrO_2 coating is the potential choice to improve the cycling stability and conductivity of MnO_2 electrode.

Acknowledgements

This project is supported by National Natural Science Foundation of China (No. 21076143), by the key technologies R & D program of Tianjin (15ZCZDSF00160), by the Basic Research of Tianjin Municipal Science and Technology Commission (13JCYBJC20100), by Tianjin Municipal Science and Technology Xinghai Program (No. KJXH2014-05), by China Scholarship Council (No: 201406255018).

Reference

1 J. R. Miller and P. Simon, *Science*, 2008, **32**, 651-652.

2 G. P. Wang, L. Zhang and J. J. Zhang, *Chem. Soc. Rev.*, 2012, **41**,797-828.

3 G. Jiang, M. Y. Zhang, X. Q. Li and H. Gao, *RSC Adv.*, 2015, **85**,69365-69370.

4 G. A. Snook, P. Kao and A.S. Best, *J. Power Sources*, 2011, **196**, 1-12.

5 G. H. Yu, X. Xie and L. J. Pan, *Nano Energy*, 2013, **2**, 213-214.

6 Y. Hou, Y. W. Cheng and T. Hobson, *Nano Lett.*, 2010 **10**, 2727-2733.

7 Y. S. Qudaih, A. A. Elbaset and T. Hiyama, *Electrical Power and Energy Systems*, 2011, **33**, 43-54.

8 C. X. Gu, M. Wang, T. Chen, X. W. Lou and C. M. Li, *Adv. Energy Mater.*, 2011,**1**, 736-741.

9 X. Lu, T. Zhai, X. Zhang, Y. Shen, L. Yuan and B. Hu, *Adv. Mater.*, 2012, **24**, 938-944.

10 L.H. Bao, J.F. Zang and X. D. Li, *Nano Lett.*, 2011, **11**, 1215-1220.

11Y. C. Hsieh, K.T. Lee, Y. P. Lin, N. L. Wu and S. W. Donne, *J. Power Sources*, 2008, **177**, 660-664.

12 J. K. Chang, M. T. Lee and W. T. Tsai, *J. Power Sources*, 2007, **166**, 590-594.

13 S. C. Pang, M. A. Anderson and T. W. Chapman, *J. Electrochem. Soc.,* 2000, **147**, 444-450.

14 S. C. Pan and M. Anderson, *J. Mater. Res.*, 2000, **15**, 2096-2106.

15 R. N. Reddy and R. G. Reddy, *J. Power Sources*, 2003, **124**, 330-337.

16 X. W. Yu and S. Licht, *J. Power Sources*, 2007, **173**, 1012-1016.

17 K. A. Walz, J. R. Szczech, A. N. Suyama, W. E. Suyama, L. C. Stoiber, W. A. Zeltner, et al, *J. Electrochem. Soc.,* 2006, **153**, A1102-A1107.

18 S. Licht, X. W. Yu and Y. F.Wang, *J. Electrochem. Soc.*, 2008, **155**, A1–A7.

19 S. Licht, X. W. Yu, D. Zheng, *Chem. Comm.*, 2006, **41**, 4341–4343.

20 P. Li, I. W. Chen and J. E. Penner-Hahn, *Phys. Rev. B.*, 1993, **48**, 10063-10073.

21 J. C. Ray, R. K. Pati and P. Pramanik, *J. Eur. Ceram. Soc.*, 2000, **20**, 1289-1295.

22 A. Ghosh, A. K. Suri and M. Pandey, *Mater. Lett.*, 2006, **60**, 1170-1173.

23 Y. Q. Zhang, G. D. Zhang, T. D. Du, *Electrochim. Acta*, 2011, **56**, 1159-1163.

24 Y. Q. Zhang, X. H. Zhao, S. M. Zhang, G. D. Zhang and S. M. Liu, *Appl. Energy*, 2012, **99**, 265-271.

25 H. P. Klug, L. E. Alexander, 2nd Edition, New York: Wiley, 1974, 554-557.

26 K. Sachin, B. Snehasis, S. Jitendra, and K.O. Animesh, J. Alloys Compd., 2015, 649, 348-356.

27 W. F. Wei, X. W. Cui, W. X. Chen and D. G. Ivey, J. Power Sources, 2009, 186, 543-550.